Static friction at fractal interfaces

Dorian A.H. Hanaor *, Yixiang Gan, Itai Einav

School of Civil Engineering, University of Sydney, NSW 2006, Australia

ARTICLE INFO

ABSTRACT

Tribological phenomena are governed by combined effects of material properties, topology and surface-chemistry. We study the interplay of multiscale surface structures with molecular-scale interactions towards interpreting static frictional interactions at fractal interfaces. By spline-assisted-discretization we analyse asperity interactions in pairs of contacting fractal surface-profiles. For elastically deforming asperities, force analysis reveals greater friction at surfaces exhibiting higher fractality, with increasing molecular-scale friction amplifying this trend. Increasing adhesive strength yields higher overall friction at surfaces of lower fractality owing to greater true-contact-area. In systems where adhesive-type interactions play an important role, such as those where cold-welded junctions form, friction is minimised at an intermediate value of surface profile fractality found to be around 1.3–1.5. Results have implications for systems exhibiting evolving surface structures.

Introduction

A meaningful micromechanical understanding of static friction and the ability to interpret its dependence on parameters of surface structure, surface chemistry, bulk material properties and environmental conditions is sought after in an extensive range of applications including granular materials [1,2], electro mechanical devices [3], structural components [4] and across the broader field of applied mechanics.

In earlier approaches to the problem, static friction was considered to arise through the simple mechanical interactions of micro-scale asperities at contacting surfaces [5,6]. The broadly observed linear dependence of frictional force on normal load of the Amontons Coulomb theory was often assumed to result from the presence of unseen surface features with a characteristic slope of α such that the coefficient of static friction follows $\mu_S = \tan\alpha$ [7]. Considering the significantly lower value of the true contact area relative to the apparent or nominal contact area, alternative approaches have considered friction arising from the shearing or debonding (cooperative or otherwise) of chemically bonded or welded junctions occurring at the regions of true contact [8–11]. A linear relationship between the total area of true contact and the applied load at an interface is ubiquitously found from numerical and experimental analyses and is indeed often utilised as a benchmark to ascertain the effectiveness of contact mechanics models [12–17]. This is understood to arise as the result of asperity

hierarchies in elastically deforming surfaces[18], and following this rationale the typical linear Amontons-Coulomb behaviour can be said to arise through shearing or debonding of these regions, which are assumed to exhibit a constant shear strength [19]. A more inclusive representation of the origins of frictional interactions is given by understanding this as an integration of structural and molecular interactions across a range of scales as described by Bowden and Tabor [20–23].

While for most purposes a constitutive understanding of frictional behaviour as captured by the Amontons-Coulomb theory is sufficient, we frequently seek to gain a fundamental insight into the complex multi-scale and multi-physics interplay between surface structure, physico-chemical properties of materials and resulting frictional interactions [24]. This is of particular importance in multi-body systems such as granular materials, in small scale applications such as micro-electromechanical systems (MEMS), as well as in conditions of low loads where the resistance to shear, as has been often observed, may not exhibit linear dependence on normal forces [25,26]. Importantly, couplings between structure and physico-chemical interactions at surfaces are of significance in systems exhibiting surface evolution and/or changing surface chemistry through changing environmental conditions or other time-dependant phenomena [27–29].

Molecular scale contributions to frictional interactions have been analysed in a range of materials and system configurations. Applying to the scale below that of measurable asperity structures, broadly this regime of effect can be divided into normal load dependant behaviour, which can be considered as atomic or molecular friction [10,30–34], and contact area dependant resistance to shear generally considered as junction shear strength,

* Corresponding author. Tel.: +61 404 188810.
E-mail address: dorian.hanaor@sydney.edu.au (D.A.H. Hanaor).

contact bonding or adhesion [35–38]. These interactions have been studied using nanoscale experimental tools including friction force microscopy applied to atomistically flat surfaces [39,40]. Data acquired through friction force microscopy is frequently interpreted using the Prandtl-Tomlinson model, which correlates surface structure with frictional behaviour and the occurrence of stick slip [41,42]. Although highly significant in the field of tribology and atomic force microscopy (AFM), this model is limited to kinetic conditions where a localised body is traversing a rough surface, and is thus of limited applicability to the interpretation of frictional interactions in static conditions [43].

Various studies have investigated the dependence of frictional phenomena on parameters of mean surface roughness (R_A) and other surface roughness descriptors [44,45]. Additionally, material properties and surface profile characteristics are often combined to give the indicative parameters such as the Plasticity Index, ψ, defined using parameters of hardness, asperity height distribution and asperity shape [46–48]. These studies have generally been constructed on the basis of a single distribution of asperity heights with assumed spherical features. However, naturally occurring surfaces tend to exhibit asperities at multiple scales in a fractal geometry exhibiting statistical self-similarity [49–52] and thus in recent years the fractal nature of surfaces has become a significant aspect in the field of experimental and computational surface analysis and contact mechanics [53–56]. The importance of considering surface fractality in contact mechanics can be explained by the tendency of first order roughness descriptors to be dominated by highest level features, while second order descriptors, such as mean slope or curvature, are dominated by the finest scales of surface features.

Using conventional finite element analysis (FEA) [38,57,58], Molecular Dynamics (MD) [33,59] and discrete element methods [60,61], challenges arise in the computationally efficient modelling of fractal surfaces and their contact mechanics, owing to the difficulties in capturing multiple scales in a single framework. Moreover, a significant majority of studies involving the contact mechanics of fractal surfaces have employed simplifications of rough to flat contact, limiting their applicability for studies towards static friction. In the present work we examine static friction occurring at interfaces of fractal surfaces in mutual contact as shown in Fig. 1, using a method based on spline assisted asperity discretisation.

2. Methods

2.1. Generation of fractal surface profiles

Static interactions between pairs of simulated fractal surfaces that are representative of engineering surfaces, such as those shown in Fig. 1, are considered where both surfaces are generated using the same value of fractality as described by the fractal dimension, D_f. To avoid the dominance of a small number of the highest surface features, rather than simulate a single pair of very long surfaces, simulations were carried out with repetition where two-dimensional fractal surface profiles of 1.5×10^5 (x,y) points were repeatedly generated (100 repetitions) and analysed with results averaged across the repetitions for each surface condition studied. With surface profiles of 40 μm in length, the finest features are thus equivalent to 2.67n Å, a figure which is towards the lower end of values typical of the separation between lattice planes in many crystalline materials.

In similarity to previously reported work, fractal profiles at each repetition r (from $r=1$ to $r=100$) were generated through a method based on the Ausloos–Berman variant of the Weirstrass
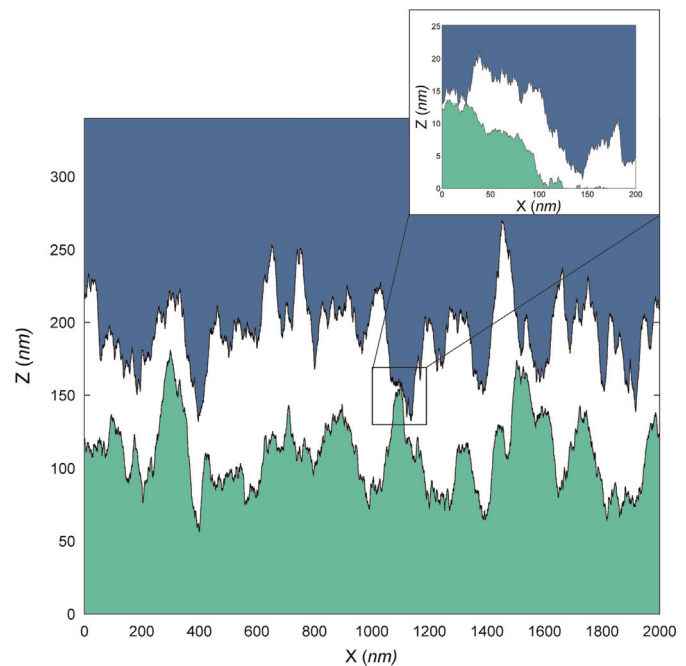

Fig. 1. Two approaching fractal surfaces showing a hierarchical structure typical of natural surfaces, as simulated in the present work.

Mandelbrot function [55,62,63].

$$y_{(x)} = L^{(4-2D_f)} \ln \gamma \sum_{m=1}^{M} \sum_{n=1}^{n \max} \gamma^{2(n-1)(D_f-2)}$$
$$\left\{ \cos \varphi_{m,n,r} - \cos \left[\frac{2\pi\gamma^{n-1}x}{L} \cos \left(-\pi\frac{m}{M} \right) + \varphi_{m,n,r} \right] \right\} \quad (1)$$

The fractal dimension of surface profiles $D_f \in (1,2)$ relates to the scale variance of the surface structure as described by its surface roughness power spectrum [64]. Hence through methods applied here $D_f=1$ corresponds to a smooth continuous quasi-random curve and $D_f=2$ corresponds to a hypothetical area filling profile, within constraints of the simulation resolution. The effect of varying fractality is illustrated by representative profile sections shown in Fig. 2. In the present work, for force evaluation we considered the D_f values between 1 and 1.7 as this interval represents the range most relevant for real material surfaces, while the use of surface profiles exhibiting higher fractal dimensions would be only of theoretical interest. In contrast to the determination of fractal parameters from real surfaces, the simulation of surface profiles following the present method is independent of the profile amplitude which is scaled to a selected height.

As with previous work, a stochastic length parameter, L, has been included in Eq. (1) to account for higher level surface features, which are present with typical wavelength. In real surfaces the term L represents a characteristic macro-asperity spacing such as that which may arise from a granular structure. The effect of varying the parameter L is illustrated by the 1 μm profile sections shown in Fig. 3. The profile used in contact simulations, with nominal lengths of 40 μm, were scaled in the y-direction to yield a consistent amplitude of asperities of 0.1 relative to the stochastic length parameter. In a separate set of simulations, the amplitude was varied to investigate effects of asperity aspect ratio. The parameter γ represents the density of frequencies used to construct the fractal profile, which on the basis of reported methods is appropriately assigned as 1.5 [65–67]. For upper and lower surfaces the set of randomised phase angles ϕ is given by a uniform distribution of size $M \times n_{max} \times r_{max}$. $\phi_{m,n,r} = U(0, 2\pi)$. In the present
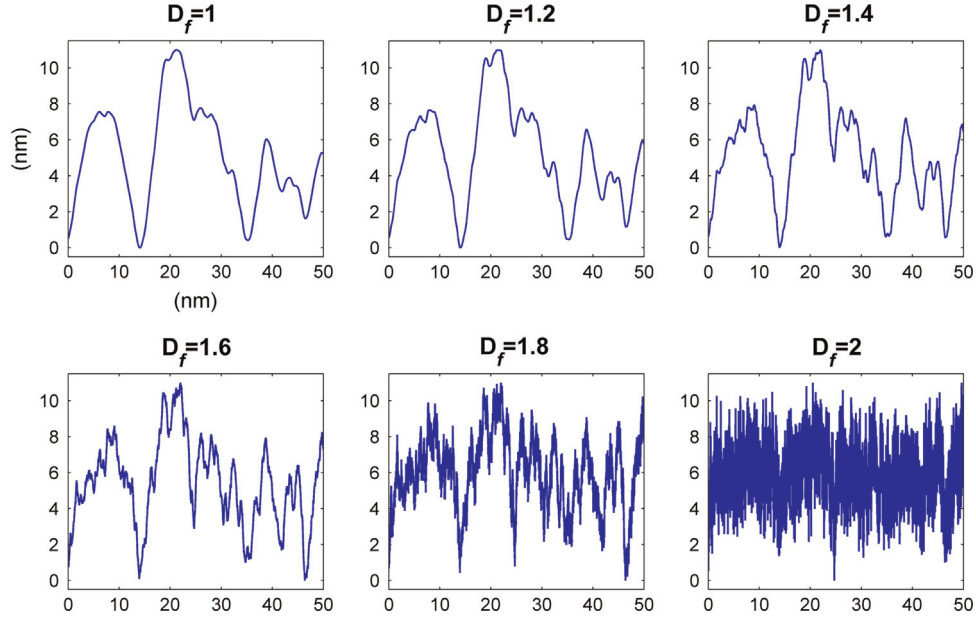
Fig. 2. Representative surface profiles over lengths of 5L, with constant roughness ($R_A = 1$), and varying D values.
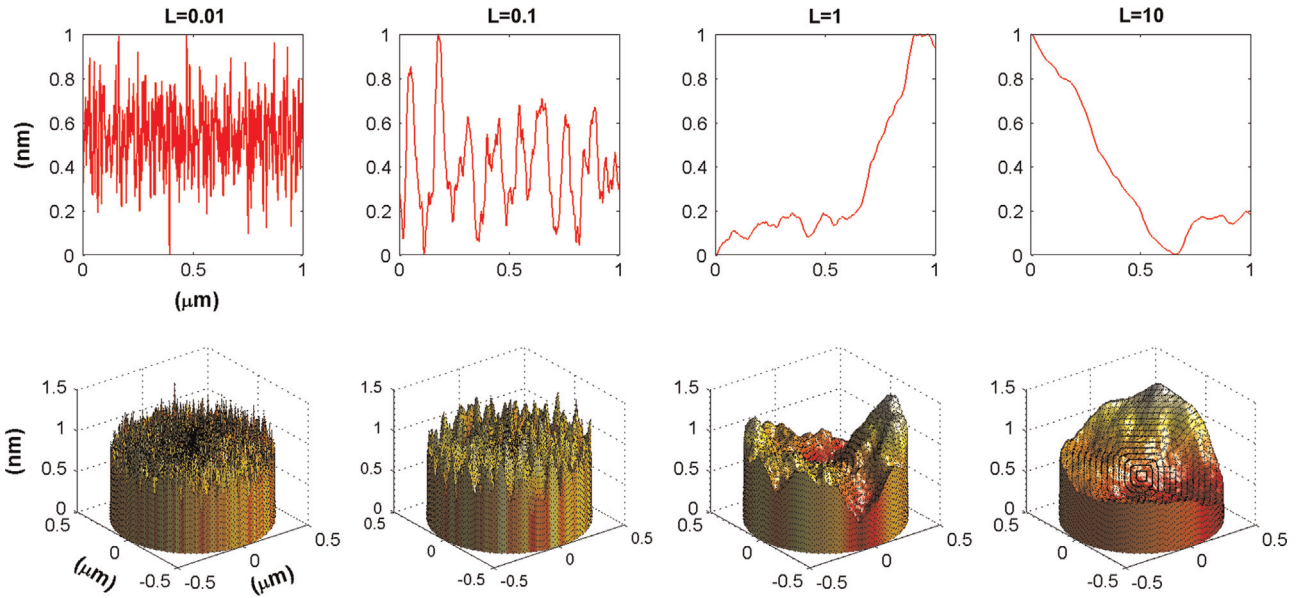

Fig. 3. Effect of the stochastic length parameter (L) in the simulation of 2D fractal profiles (upper) and equivalent 3D surfaces (lower).

work M and n_{max} values of 40 were chosen as these were found to give sufficiently randomised surfaces, while the number of repetitions, r_{max}, is 100 as described.

To represent macroscopically flat interfaces, repeatedly simulated pairs of fractal surface profiles were generated over a length of 40L, to give on average 40 largest scale surface features per surface per repetition. To yield dimensional results (mN, μm) the value of L is assigned as 1 μm. Surfaces of varying fractality were studied over 100 repetitions. For each repeated contact scenario studied, two simulated surfaces, upper and lower, were generated with differing ϕ sets. These ϕ sets were preserved across all fractalities studied, varied from $D_f = 1.0$ to 1.7, in order to yield macroscopically similar profiles comparable to the profiles illustrate in Fig. 2. Surface profiles are assumed to be of unity thickness with micron dimensions used in order to show results pertinent to macroscopically flat engineering surfaces which typically exhibit roughness features in this scale regime.

2.2. Spline assisted asperity discretization

Owing to the non-differentiability of fractal surfaces, surface normals and radii of curvature at discrete surface points on simulated profiles are extracted using a method of spline assisted asperity discretization (SAAD) as applied previously [68]. This allows the global contact problem to be treated as a series of local contact events. Following this method surface points are discretised using a cubic spline interpolation passing through all simulated points to describe surface features in terms of meaningful values of surface orientation and curvature radii, determined from the spline derived piecewise polynomial, $f(x)$ at individual points (x_i, y_i)

$$\vec{n}_i = \left[\pm f'(x_i)\left(f'(x_i)^2 + 1\right)^{-0.5}, \quad \mp \left(f'(x_i)^2 + 1\right)^{-0.5} \right]^T \quad (2)$$

$$R_i = \frac{\left(1 + f\,'(x_i)^2\right)^{3/2}}{f\,'(x_i)}, \quad \vec{O}_i = \vec{x}_i - R_i \vec{n}_i \tag{3}$$

Here $\vec{n}_i$ is the surface normal represented by a vector of unity magnitude the orientation of which varies depending on whether the surface is upper or lower in the contact event. R_i is the local surface radius and assumes negative values for concave regions of the surfaces and tends towards infinity for a perfectly flat surface, while $\vec{O}_i$ represents the position vector of local sphere centres.

Following this discretisation, points involved in contact events are treated as Hertzian spheres where the relative positions of sphere centres for contacting asperities are utilised in order to compute the magnitude and orientation of localised normal and tangential forces as well as the areas of individual contact patches at active asperities. Forces and areas are then summed to yield global forces acting on the surface, which is assumed not to exhibit macroscopic flexure, as well as total true contact area. A schematic illustration is given in Fig. 4.

2.3. Force evaluation

In the presently applied method we examine a static snapshot of discretised asperity interactions in normal and tangential orientations. Contact detection involves initially the identification of points satisfying the condition $y_i^u \leq y_i^l$, where superscripts u and l denote upper and lower surfaces. Secondly for each contact point a contact normal, in the form of a vector of unity magnitude $\vec{n}_i^c$, and a contact centre c_i^c are evaluated.

$$\vec{n}_i^c = \frac{\vec{O}_i^u - \vec{O}_i^l}{\left|\vec{O}_i^u - \vec{O}_i^l\right|} = \frac{\vec{X}_i}{\left|\vec{X}_i\right|}, \quad \vec{c}_i^c = \frac{\vec{X}_i}{2} - \frac{R_i^u - R_i^l}{2}\vec{n}_i^c \operatorname{sgn}\left(R_i^u R_i^l\right) \tag{4}$$

Here $\vec{X}_i$ is the vector separation of the contacting sphere centres. It should be noted that the contact normals differ from the surface normals defined by SAAD.

Thirdly, as the grid of the simulated surface is of sufficiently high resolution to exhibit locally smooth topology, the number of actual contacting asperities is lower than the count of intruding grid points satisfying the aforementioned condition. For this reason, to avoid the force evaluation at single contacting asperities being represented by fluctuating numbers of spheres we exclude

Fig. 4. Diagram of forces, normals and incremental displacements at a single contact point.

contacts between spheres on opposing surfaces occurring at points distant from their respective surface profile coordinates and thus avoid mesh dependence and discontinuities in force evaluation. Thus contact points are accepted only when their centres are located within the domain defined by

$$x_i^c \in \left[x_i - \frac{\Delta x}{2}, \quad x_i + \frac{\Delta x}{2}\right] \tag{5}$$

where x_i^c is the global x-axis coordinate of the contact centre and Δx is the grid x-spacing of the surface-profiles. In the absence of this criterion, a single peak to peak contact point may be represented by a large number of spheres corresponding to distant points, and consequently yield an erroneously high local normal force.

At individual accepted contact points local normal forces and individual contact areas are resolved following the the two dimensional Hertzian solution for elastic spheres [69,70]. However, alternative solutions can readily be incorporated to accommodate divergent surface mechanics and material behaviour including asperity elasto-plasticity [71]. In the presently reported methodology an effective elastic modulus of $E^* = 10$ GPa is utilised in order to yield dimensional results relevant to engineering surfaces.

2.4. Friction evaluation

We aim to quantify static friction arising from interactions of asperities in simulated interfaces of fractal surfaces, and to gain insights into relationships between surface structure and friction. Additionally we incorporate parameters meaningfully representing molecular friction and adhesion to account for known physico-chemical interactions at material surfaces and examine the interplay between these parameters. In materials these interactions are governed by localised properties including surface crystallography, surface chemistry, the presence of adsorbates and electrostatic interactions.

The contact of atomistically smooth surfaces involves frictional interactions despite the absence of measureable asperities. These interactions, referred to varyingly as atomic, molecular, phononic or interface friction arise from intermolecular forces, electronic and van der Waals interactions at interfaces and are profoundly affected by the presence of adsorbed species [72–74]. Additionally, limitations to our ability to characterise asperity structures mean that surfaces may exhibit roughness features smaller than the scale which we are able to measure or meaningfully simulate. In the present study of rough to rough contact conditions these considerations are addressed by including a molecular/atomic friction coefficient, μ_0, studied over the interval 0.1 to 1, to account for all interactions at scales below the scale of simulated asperities in the present work. It is assumed that this atomic friction coefficient is homogenous at all contact points regardless of height, orientation or contact length, although in natural surfaces variations in surface chemistry and crystallographic orientation would be expected to bring about inhomogeneities in this parameter. Following this the maximal locally tangential force that can be borne at an individual contact patch is given as

$$\vec{F}_i^t = \mu_0 \left|\vec{F}_i^n\right| \vec{t}_i^c \tag{6}$$

where $\vec{t}_i^c$ is a unit vector in the local tangential orientation.

Finally the global coordinate system force balance is examined by summing the components of individual local forces at contact points in the global normal and tangential directions. In the global tangential direction we only sum forces corresponding to contact points where $F_i^{n,T} < 0$, that is to say where asperity interactions
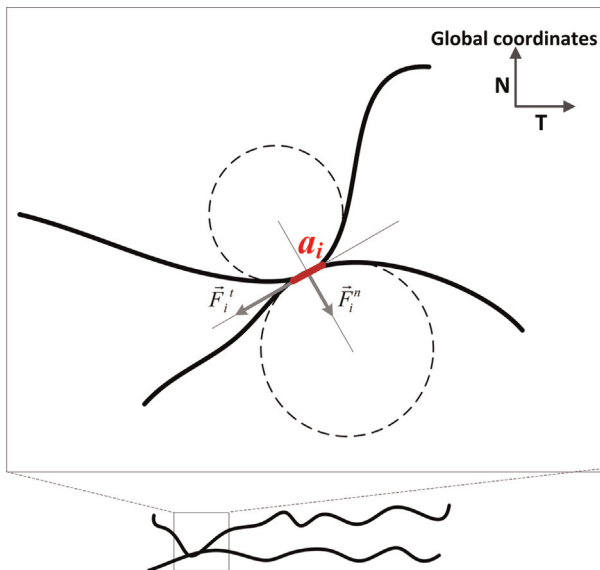
oppose an applied shear strain:

$$F_N = \sum \left(F_i^{n,N} + F_i^{t,N} \right), \quad F_T = \sum \left(F_i^{n,T} + F_i^{t,T} \right) \tag{7}$$

where $F_i^{n,N}$ and $F_i^{n,T}$ represent, respectively, the global normal and global tangential components of the local normal force acting at contact point i. Inherent to this methodology is the simplified assumption that through processes of deformation or micro-slip [75,76] asperity contacts opposing shear reach their maximum local tangential force while asperities that do not oppose shear become unloaded.

2.5. Adhesion type interactions

The forces contributing to observed frictional phenomena across multiple scales arise from combined mechanical, electrostatic and molecular mechanisms. These have been investigated in recent years in a range of publications [59,77–80]. In a constitutive approach at the finest scales frictional stress τ_f can be described by a load dependant component α (equivalent to μ_0), and a material-interface-dependant adhesive shear stress τ_0 such that $\tau_f = \tau_0 + \alpha P$[81,82]. With P being the contact pressure that is the sum of applied and capillary-induced components. The relative significance of the material and load dependant components is strongly influenced by the contact profile and fractality of surface structures.

Consequently for asperities involved in resistance to shear, we include in our force evaluation of frictional forces an adhesive component of varied significance, F_i^A. This is evaluated as $\overrightarrow{F}_i^A = \tau_0 A_i \overrightarrow{t}_i^c$, with overall friction evaluated as $F_T = \sum \left(F_i^{n,T} + F_i^{t,T} + F_i^{A,T} \right)$.

Similarly, normal forces are evaluated including the normal component of adhesive forces in the global normal orientation. In the present work we studied τ_0 values of 500 KPa, 10 MPa, 100 MPa and 200 MPa, to represent a range of natural adhesive interactions, such as those that might arise from can der Waals forces, micro-capillary forces or cold welded junctions of engineering alloys [80,83–85]. Additionally we apply the current methods without the inclusion of τ_0 and the contact area dependant forces that arise from this parameter.

For varied conditions of fractality (D_f), atomic friction (μ_0) and adhesive shear strength (τ_0) the macroscopic friction coefficient is evaluated in a straightforward manner by the overall ratio of F_T to F_N in the global coordinate system.

3. Results

3.1. Frictional interactions of fractal surfaces

From the SAAD based analysis of contact events between pairs of amplitude-normalised fractal rough surfaces, conducted to a constant level of normal displacement, it is found that the evolution of true contact area with applied normal load closely follows a linear relationship, with some deviation at low normal loads. Results here are dimensional owing to the assumption of a profile of 1 μm thickness and 40 μm in total length, and an effective modulus of 10 GPa. This is chosen for illustrative purposes and non-dimensionalisation is readily possible. The resolution level used here is sufficiently high to allow the representation of the scale regime of realistic macroscopically flat engineering surfaces (surfaces with features at length scales from 10^{-3} m to 10^{-10} m). In the present method the dimensional values of true contact area and normal force are somewhat affected by decreasing sampling resolution with this effect being more prominent for surfaces of higher fractality. Overall analysis results are sufficiently robust. Coarsening the sampling grid in the horizontal orientation has a

similar effect to decreasing D_f and on the basis of the analysis of 100 surface interactions, decreasing the grid resolution used here by a factor of 10 was found to result in contact area overestimation within 0.3% and underestimation of F_N within 0.6% (relative to full resolution results) for surfaces with $D_f = 1.3$ at maximum displacement, with these discrepancies respectively increasing to ranges of 2.2% and 3.9% for $D_f = 1.7$. The maximal F_N values obtained differ with D_f as the simulations were displacement driven. Overall the observed linear behaviour of true contact area is expected for hierarchical surface structures as predicted by Archard [18] and as confirmed in a range of experimental studies and by computational methods including boundary element method (BEM) [86] and FEA [57,87,88]. The results shown in Fig. 5 were acquired from repeatedly simulated profiles with conditions of $\tau_0 = 10$ MPa and $\mu_0 = 0.4$, although these two parameters have a comparatively insignificant effect on the behaviour of true contact area and normal contact stiffness with applied normal load.

Following the methods described for the evaluation of macroscopically observed friction, the significance of loading conditions and surface structure are studied for a range of systems differentiated by parameters of their molecular scale friction coefficient (μ_0) and adhesive shear strength at regions of true contact (τ_0). As with all studies here, data points are established by averaging over the repeated generation of 100 surface profile pairs, with results shown in Fig. 6. Although applied in a simplified manner in the present method, these two parameters are intrinsically linked to conditions of surface chemistry, temperature and environment and vary greatly with material type, surface orientation and environmental conditions. Here we examine μ_0 values in the region 0.1–1.0, which covers the range of atomic friction coefficients typically reported for the study of atomistically flat surfaces [89,90]. Adhesive (load independent) interactions were studied by applying a shear strength τ_0 in the regime of 500 KPa to 200 MPa. As expected owing to the low value of true contact area relative to nominal contact, little difference was found between conditions of $\tau_0 \leq 1$ MPa, and conditions where adhesion type interactions are neglected i.e. $\tau_0 = 0$.

As higher surface slopes result greater normal forces at contact points, surfaces of greater fractality unsurprisingly exhibit a general tendency towards higher resistance to shear and a larger macroscopically observed friction coefficient shown on the right side of the plots in Fig. 6. At regions of both high surface fractality and low applied normal load, the apparent macroscopic friction
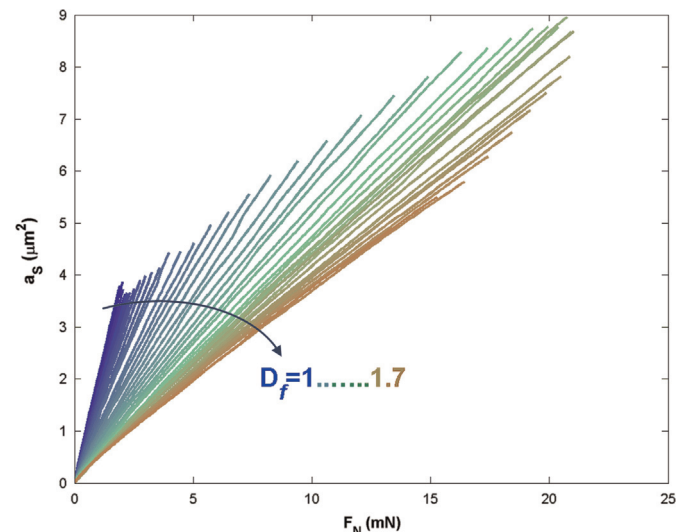
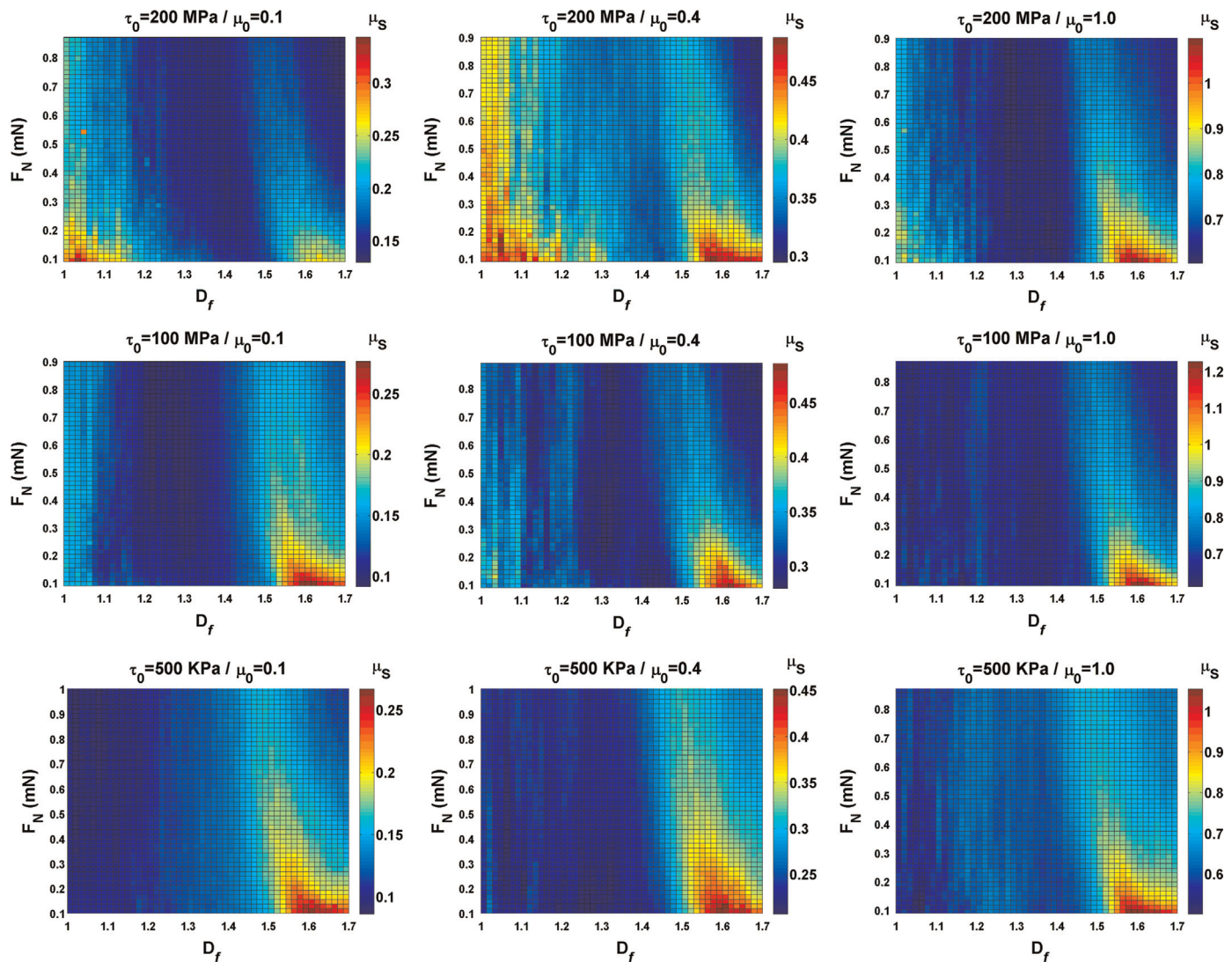**Fig. 5.** Variation of true contact area with applied normal load for simulated surface profiles generated with $D_f = 1$–1.7.

Fig. 6. Variation of macroscopic friction coefficient (μ_S, colour bars) with fractal dimension and applied normal load for conditions of different adhesive strength (τ_0) and atomic friction (μ_0). (For interpretation of the references to colour in this figure legend, the reader is referred to the web version of this article.)

tends towards higher values following a similar pattern for all studied systems shown in the bottom right corners of the plots. It is worth noting that the results here show that for particular surface structures and applied loads we expect to encounter certain conditions where the macroscopic friction is lower than the molecular scale friction coefficient. That is to say the friction coefficient may be greater at a rough interface than at an atomically flat surface having the same material properties (bulk and surface). This can be explained by the fact that, unlike completely smooth surfaces, at rough interfaces, contact events are localised to a limited number of areas. In the present method, while the normal load F_N is contributed to by forces at all asperities involved in the contact event, the maximal tangential force F_T is contributed to only by asperity contacts oriented such that they resist shear. This result is supported by experimental results from various materials where the presence of increased roughness is often found to decrease the magnitude of frictional interactions within certain regimes under given loads, although it should be noted that this has been studied with respect to dynamic interactions [91,92].

Conditions where shearing of cold welded asperity interfaces play a significant role, i.e. high τ_0 values, yield an increase in overall friction across all levels of fractality and at all applied loads,

however this trend is most evident towards low fractality and low applied normal load. Under such conditions overall friction is found to exhibit a minimum at intermediate fractal dimension values in the range ~1.3–1.5. Interestingly, this result demonstrates that for particular systems we may observe a non-monotonous variation of static friction with surface fractality. An increasingly high molecular friction coefficient naturally manifests in higher overall friction under all conditions with this being most prominent for surfaces with $D_f > 1.5$.

3.2. Aspect ratio effects

To study the effects of asperity aspect ratio on frictional interactions, the controlled amplitude was varied with respect to the stochastic length parameter L. This has the effect of governing the approximate aspect ratio of highest level asperities in terms of asperity height to asperity projection in the horizontal plane. The effects of asperity aspect ratio on static friction are illustrated by Fig. 7. In most engineering materials the aspect ratio is significantly less than 1 as asperity heights are generally significantly lower than the mean spacing (approximate wavelength) of highest level features. As with molecular scale interactions, the typical aspect ratio of asperities on macroscopically flat surfaces is highly
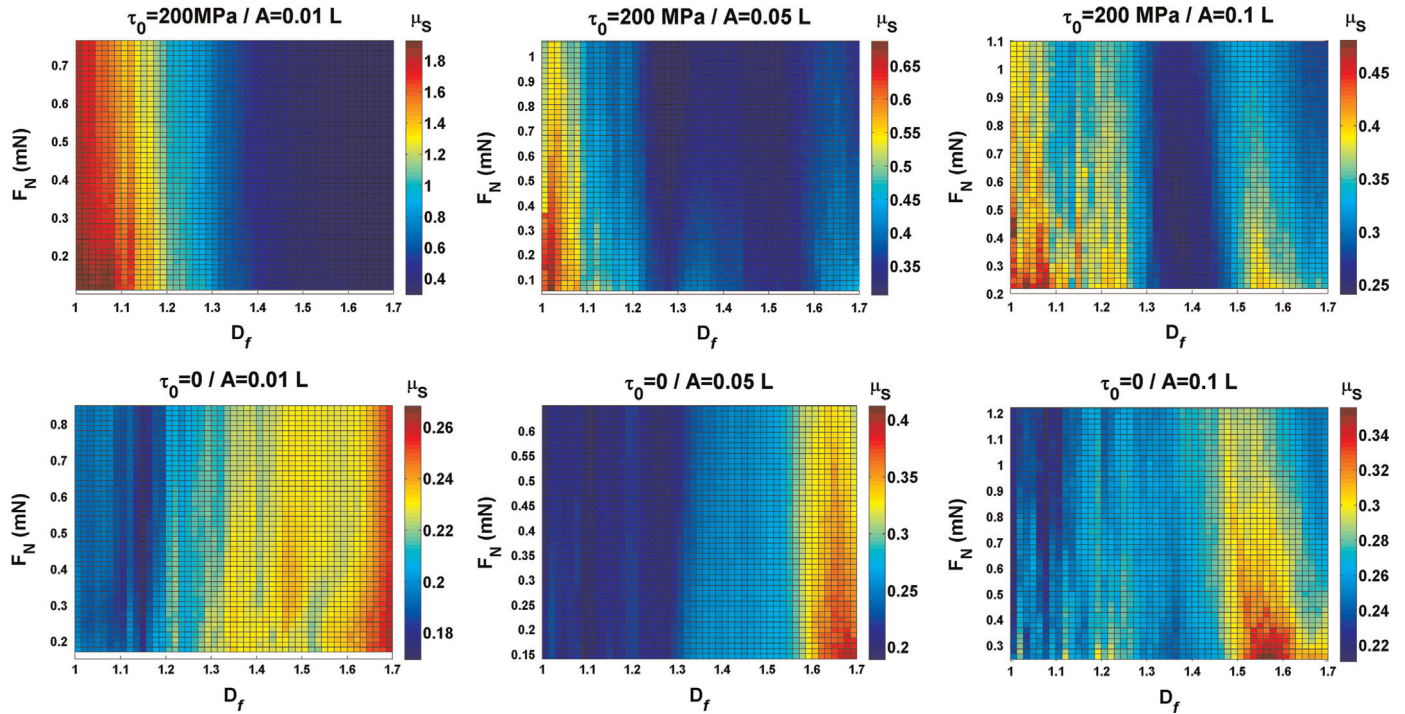
Fig. 7. Variation of macroscopic friction coefficient (μ_S, colour bars) with fractal dimension and applied normal load for different conditions of asperity aspect ratio (A) and adhesive strength (τ_0). (For interpretation of the references to colour in this figure legend, the reader is referred to the web version of this article.)

dependant on the material type, with ductile materials showing low aspect ratios while ceramics and harder alloys exhibit higher asperity peaks relative to their horizontal size [93,94].

The trend of higher static frictional strength towards regions of higher surface fractality is less prominent for surfaces with broader asperities, that is to say a lower amplitude relative to the value of *L*. This may be the result of lower surface slope values resulting in large number of contact points involved in frictional events. Moreover it can be seen that where adhesive interactions dominate the trend of higher friction at low surface fractality is more pronounced for flatter asperities, as the result of higher level of true contact area thus occurring. For surfaces dominated by contact bonding (higher adhesion) such those where static friction is assumed to arise from cold-welded junctions ($\tau_0 = 200$ MPa), it is further worth noting that with increasing relative asperity amplitudes, the friction coefficient across all surface types and loading conditions exhibits a decreasing trend. This is the result of a decreasing true contact area at a given load, as the asperity aspect ratio increases, and the relative contribution of the adhesion to the macroscopic friction coefficient decreases. This is further illustrates in Fig. 8, which shows the variation of true contact area with normal load for different sets of fractal surfaces at 3 different controlled profile amplitudes.

4. Discussion

Contact mechanics and frictional interactions between pairs of multiscale rough surfaces were evaluated using SAAD. This study employed profiles simulated using procedures for the generation of realistic fractal surfaces at resolution sufficient to capture features of solid interfaces down to molecular scales. This methodology could further be used in conjunction with surface data acquired from AFM, surface profilometry or through alternative surface simulation algorithms. The numerical results obtained were found to exhibit robustness with respect to analysis resolution. Decreasing the sampling resolution of the surface profiles
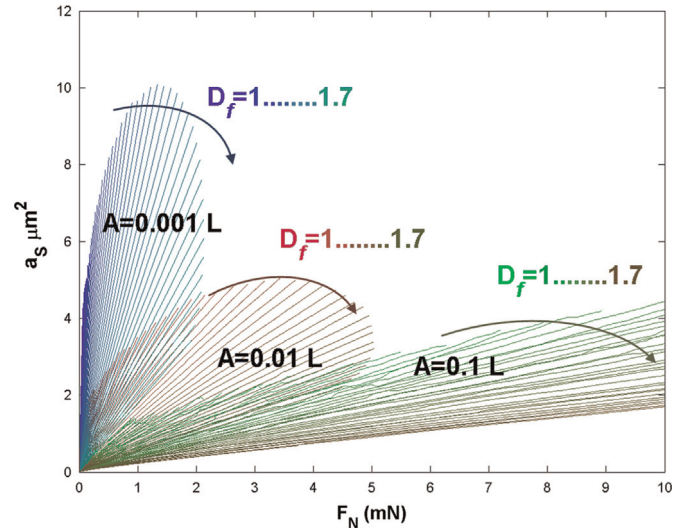

Fig. 8. Variation of true contact area (a_S) with applied normal load (F_N) for surfaces of different fractality across three data sets differed by their relative amplitudes (A).

studied yielded minor discrepancies in the evaluated contact area and forces, with these discrepancies increasing for surfaces of greater fractality. Thus the methods applied here do not necessitate the input of surface data with atomic-scale resolution, although it should be noted that the meaningful simulation or characterisation of highly fractal surfaces is improved by an ability to capture finer-scale features.

The present approach involves rough-to-rough analysis in contrast to the majority of comparable work that most often involves rough to rigid flat simplifications for the study of similar interactions. The methods employed here have the notable advantage of facilitating the examination of the integrated effects of surface structure and surface chemistry on frictional interactions at rough to rough interfaces, in a manner that is computationally efficient relative to comparable FEA methods. Despite

advantageous aspects of this model, there exist notable limitations of the presently applied approach. Importantly the present method examines a static snapshot for given structures and material parameters, and does not consider time dependant surface evolution, temperature effects on molecular scale interactions, plastic deformation of asperities and the discontinuously distributed tangential displacement of the surfaces as may occur through processes of deformation and microslip [33,75,76,95,96]. Furthermore, in studying mechanisms of bonding interactions (varied τ_0) at regions of true contact, we assume these areas to be governed by Hertzian contact mechanics whereas a more suitable approach would be to consider cold-welded regions and Hertzian regions through separate frameworks [97].

The linearity between true contact area and applied load for surfaces of varied fractality is shown in Figs. 5 and 8 and, as a commonly utilised benchmark, serves to validate the methods applied here. Although, it is likely that frameworks incorporating elasto-plastic asperity deformation would yield a more meaningful interpretation with respect to engineering materials [65]. Importantly, the SAAD method facilitates the study of contact mechanics and friction interactions in multiscale surfaces that would otherwise necessitate computationally intensive analysis. For given values of τ_0 and μ_0 and D_f the repeated analysis of contact events between two surface profiles consisting each of 1.5×10^5 points, over 100 reiterations was achieved in the order of one minute. This computationally efficient approach thus facilitates parametric studies including of a broad range of variables here chosen as fractality, adhesive strength, molecular friction and surface amplitude. The execution of such a methodology in a finite element framework would be highly problematic owing to the large number of elements that would be necessary in order to mesh the structures adequately with statistically significant surface generation. Alternative approaches to the computational description of interfaces have utilised principal component analysis, Fourier transforms or other mathematical formulations to represent periodic multiscale surface profiles [98]. However, this approach, while enabling computationally efficient parametric studies, may not meaningfully capture the nature of real surfaces in terms of random fractal asperity structures.

Results demonstrate the interplay between parameters of applied load, surface fractality and molecular mechanisms of friction. These relationships are evident of the necessity to consider cross scale surface structures and surface chemistry in tandem with loading conditions to evaluate the development of frictional interactions, which for certain systems may indeed exhibit a non-monotonous variation with surface fractality. The results of the presently applied methods have significance towards understanding the evolution of force networks in multi-body systems and under conditions of low normal load, where non-linearity between normal load and frictional forces may be observed, and evolving surface structure and interface chemistry can fundamentally alter bulk system behaviour. Numerous simplifications are involved in the present work, such as an atomic/molecular friction coefficient that is independent of load and material orientation, where in fact friction at atomistically flat interfaces is generally reported to vary with load and crystallographic orientation of the surfaces in contact, with negative friction occurring under certain conditions [99].

On the basis of the present method, for surfaces of greater fractality, we predict a higher macroscopically observed friction coefficient, with this trend diminishing for surface conditions that are conducive to bonding and the formation of adhered junctions. This trends are consistent with behaviour experimentally observed in certain systems [100]. Additionally, an increase in lowest scale friction occurring through molecular interactions, as represented by μ_0, produces an increase in the magnitude of macroscopic

friction for all surface structures studied, with this trend expected to be somewhat greater for surfaces of greater fractality. Lower asperity aspect ratios, which generally are found following polishing treatments, naturally give rise to a higher true contact area under a given applied load, increasing frictional forces for surface of lower fractality and leading to greater significance of potential adhesive interactions.

It is worth noting that at rough interfaces the magnitude of load-independent bonding strength may paradoxically depend on the nature of loading history. This is often the case for rough metallic interfaces where a high asperity-localised load may facilitate metal–metal bonding while oxide or hydration-passivated layers exhibit weak van der Waals mediated interactions. For this reason the assumption that the value of τ_0 is constant at all contact regions merits revision in future work.

5. Conclusions

We have developed and demonstrated the application of a computationally efficient method for the study of rough to rough surface interactions towards the prediction of static frictional forces on the basis of discretisation of a hierarchical surface structure. The present method involves simplifications in terms of surface mechanics and phyisco-chemical surface interactions but nonetheless facilitates the interpretation of the dependence of frictional forces on parameters of surface fractality, molecular scale friction and adhesive type interactions. Results show that under certain conditions friction may be minimised at an intermediate regime of surface fractality and further confirm that the macroscopically observed friction coefficient for a rough surface in a particular system can be lower than the friction coefficient of an atomically smooth surface of the same material.

In conjunction with the characterisation of specific material surface interactions and the evaluation of multi-scale surface structures, the methods developed have the potential to inform the modification of surface structures towards optimisation of frictional interactions and interpretation of mechanical phenomena in multi-body and micro-scale systems.

Acknowledgements

References

[1] Nemat-Nasser S. A micromechanically-based constitutive model for frictional deformation of granular materials. J Mech Phys Solids 2000;48:1541–63.
[2] Alonso-Marroquín F, Ramírez-Gómez Á, González-Montellano C, Balaam N, Hanaor DA, Flores-Johnson E, et al. Experimental and numerical determination of mechanical properties of polygonal wood particles and their flow analysis in silos. Granul Matter 2013;15:811–26.
[3] Berman D, Krim J. Surface science, MEMS and NEMS: progress and opportunities for surface science research performed on, or by, microdevices. Prog Surf Sci 2013;88:171–211.
[4] Blau PJ. The significance and use of the friction coefficient. Tribol Int 2001;34:585–91.
[5] O'Connor J, Johnson K. The role of surface asperities in transmitting tangential forces between metals. Wear 1963;6:118–39.
[6] Student E, Rudzitis J. Contact of surface asperities in wear. Tribol Int 1996;29:275–9.
[7] Müser MH, Wenning L, Robbins MO. Simple microscopic theory of Amontons laws for static friction. Phys Rev Lett 2001;86:1295.
[8] Filippov A, Klafter J, Urbakh M. Friction through dynamical formation and rupture of molecular bonds. Phys Rev Lett 2004;92:135503.
[9] Bowden F, Rowe G. The adhesion of clean metals. Proc R Soc Lond A Math Phys Sci 1956;233:429–42.

[10] Ringlein J, Robbins MO. Understanding and illustrating the atomic origins of friction. Am J Phys 2004;72:884–91.

[11] Barry B, Tribology Milburn P. friction and traction: understanding shoe-surface interaction. Footwear Sci 2013;5:137–45.

[12] Adams G, Nosonovsky M. Contact modeling—forces. Tribol Int 2000;33:431–42.

[13] Buchner B, Buchner M, Buchmayr B. Determination of the real contact area for numerical simulation. Tribol Int 2009;42:897–901.

[14] Carbone G, Bottiglione F. Asperity contact theories: do they predict linearity between contact area and load? J Mech Phys Solids 2008;56:2555–72.

[15] Carbone G, Bottiglione F. Contact mechanics of rough surfaces: a comparison between theories. Meccanica 2011;46:557–65.

[16] Zavarise G, Borri-Brunetto M, Paggi M. On the reliability of microscopical contact models. Wear 2004;257:229–45.

[17] Zavarise G, Borri-Brunetto M, Paggi M. On the resolution dependence of micromechanical contact models. Wear 2007;262:42–54.

[18] Archard J. Elastic deformation and the laws of friction. Proc R Soc Lond A Math Phys Sci 1957;243:190–205.

[19] Barber J. Multiscale surfaces and Amontons' law of friction. Tribol Lett 2013;49:539–43.

[20] Tabor D. Junction growth in metallic friction: the role of combined stresses and surface contamination. Proc R Soc Lond A Math Phys Sci 1959;251:378–93.

[21] Tabor D. Surface forces and surface interactions. J Colloid Interface Sci 1977;58:2–13.

[22] Bowden F, Tabor D. The area of contact between stationary and between moving surfaces. Proc R Soc Lond A Math Phys Sci 1939;391–413.

[23] Ramezani M, Ripin ZM. A friction model for dry contacts during metal-forming processes. Int J Adv Manuf Technol 2010;51:93–102.

[24] Urbakh M, Klafter J, Gourdon D, Israelachvili J. The nonlinear nature of friction. Nature 2004;430:525–8.

[25] Adams GG, Müftü S, Azhar NM. A scale-dependent model for multi-asperity contact and friction. J Tribol 2003;125:700–‐8.

[26] Persson BNJ. Contact mechanics for randomly rough surfaces. Surf Sci Rep 2006;61:201–27.

[27] Somorjai GA, Li Y. Impact of surface chemistry. Proc Natl Acad Sci 2011;108:917–24.

[28] Li Q, Tullis TE, Goldsby D, Carpick RW. Frictional ageing from interfacial bonding and the origins of rate and state friction. Nature 2011;480:233–6.

[29] Goedecke A, Mock R.Transient friction effects due to variable normal load in a multi-scale asperity-creep friction model. In: Proceedings of STLE/ASME 2010 International Joint Tribology Conference: American Society of Mechanical Engineers; 2010. p. 337–9.

[30] Bhushan B, Israelachvili JN, Landman U. Nanotribology: friction, wear and lubrication at the atomic scale. Nature 1995;374:607–16.

[31] Enachescu M, Van Den Oetelaar R, Carpick RW, Ogletree D, Flipse C, Salmeron M. Atomic force microscopy study of an ideally hard contact: the diamond (111)/tungsten carbide interface. Phys Rev Lett 1998;81:1877–80.

[32] Bhushan B. Micro/nanotribology and its applications to magnetic storage devices and MEMS. Tribol Int 1995;28:85–96.

[33] Spijker P, Anciaux G, Molinari J-F. Relations between roughness, temperature and dry sliding friction at the atomic scale. Tribol Int 2013;59:222–9.

[34] Wang C, Li H, Zhang Y, Sun Q, Jia Y. Effect of strain on atomic-scale friction in layered MoS 2. Tribol Int 2014;77:211–7.

[35] Chang W-R, Etsion I, Bogy D. Static friction coefficient model for metallic rough surfaces. J Tribol 1988;110:57–63.

[36] Gao J, Luedtke W, Gourdon D, Ruths M, Israelachvili J, Landman U. Frictional forces and Amontons' law: from the molecular to the macroscopic scale. J Phys Chem B 2004;108:3410–25.

[37] Castagnetti D, Dragoni E. Adhesively-bonded friction interfaces: macroscopic shear strength prediction by microscale finite element simulations. Int J Adhes Adhes 2014;53:57–64.

[38] Castagnetti D, Dragoni E. Predicting the macroscopic shear strength of adhesively-bonded friction interfaces by microscale finite element simulations. Comput Mater Sci 2014;64:146–50.

[39] Lee C, Li Q, Kalb W, Liu X-Z, Berger H, Carpick RW, et al. Frictional characteristics of atomically thin sheets. Science 2010;328:76–80.

[40] Gnecco E, Bennewitz R, Pfeiffer O, Socoliuc A, Meyer E. Friction and wear on the atomic scale. Nanotribology and nanomechanics II. Berlin: Springer-Verlag; 2011. p. 243–92.

[41] Müser MH. Velocity dependence of kinetic friction in the Prandtl–Tomlinson model. Phys Rev B 2011;84:125419.

[42] Jansen L, Hölscher H, Fuchs H, Schirmeisen A. Temperature dependence of atomic-scale stick-slip friction. Phys Rev Lett 2010;104:256101.

[43] Popov V, Gray J. Prandtl-Tomlinson model: history and applications in friction, plasticity, and nanotechnologies. ZAMM – J Appl Math Mech (Z Angew Math Mech) 2012;92:683–708.

[44] Karpenko YA, Akay A. A numerical model of friction between rough surfaces. Tribol Int 2001;34:531–45.

[45] Menezes PL, Kailas SV. Effect of surface roughness parameters and surface texture on friction and transfer layer formation in tin–steel tribo-system. J Mater Process Technol 2008;208:372–82.

[46] Greenwood J, Williamson J. Contact of nominally flat surfaces. Proc R Soc Lond A Math Phys Sci 1966;295:300–19.

[47] Kogut L, Etsion I. A static friction model for elastic-plastic contacting rough surfaces. Trans-Am Soc Mech Eng J Tribol 2004;126:34–40.

[48] Kanji M. The relationship between drained friction angles and Atterberg limits of natural soils. Geotechnique 1974:24.

[49] Go J-Y, Pyun S-I. Fractal approach to rough surfaces and interfaces in electrochemistry. Modern aspects of electrochemistry. Springer; 2006. p. 167–229.

[50] Hasegawa M, Liu J, Okuda K, Nunobiki M. Calculation of the fractal dimensions of machined surface profiles. Wear 1996;192:40–5.

[51] Mandelbrot BB. The fractal geometry of nature. London: Macmillan; 1983.

[52] Hanaor DAH, Ghadiri M, Chrzanowski W, Gan Y. Scalable surface area characterisation by electrokinetic analysis of complex anion adsorption. Langmuir 2014;30:15143–52.

[53] Avnir D, Farin D, Pfeifer P. Molecular fractal surfaces. Nature 1984;308:261–3.

[54] Buzio R, Boragno C, Biscarini F, De Mongeot FB, Valbusa U. The contact mechanics of fractal surfaces. Nat Mater 2003;2:233–7.

[55] Yan W, Komvopoulos K. Contact analysis of elastic-plastic fractal surfaces. J Appl Phys 1998;84:3617–24.

[56] Putignano C, Afferrante L, Carbone G, Demelio GP. A multiscale analysis of elastic contacts and percolation threshold for numerically generated and real rough surfaces. Tribol Int 2013;64:148–54.

[57] Poulios K, Klit P. Implementation and applications of a finite-element model for the contact between rough surfaces. Wear 2013;303:1–8.

[58] Bryant MJ, Evans HP, Snidle RW. Plastic deformation in rough surface line contacts—a finite element study. Tribol Int 2012;46:269–78.

[59] Harrison J, White C, Colton R, Brenner D. Molecular-dynamics simulations of atomic-scale friction of diamond surfaces. Phys Rev B 1992;46:9700.

[60] Jerier J, Molinari J. Normal contact between rough surfaces by the discrete element method. Tribol Int 2012;47:1–8.

[61] Avlonitis M, Kalaitzidou K, Streator J. Investigation of friction statistics and real contact area by means of a modified OFC model. Tribol Int 2014;69:168–75.

[62] Ausloos M, Berman D. A multivariate Weierstrass-Mandelbrot function. Proc R Soc Lond A Math Phys Sci 1985;400:331–50.

[63] Saupe D. Algorithms for random fractals. The science of fractal images. Berlin: Springer-Verlag; 1988. p. 71–136.

[64] Geike T, Popov VL. Mapping of three-dimensional contact problems into one dimension. Phys Rev E 2007;76:36710.

[65] Morag Y, Etsion I. Resolving the contradiction of asperities plastic to elastic mode transition in current contact models of fractal rough surfaces. Wear 2007;262:624–9.

[66] Majumdar A, Tien C. Fractal characterization and simulation of rough surfaces. Wear 1990;136:313–27.

[67] Ciavarella M, Delfine V, Demelio GA. "re-vitalized" Greenwood and Williamson model of elastic contact between fractal surfaces. J Mech Phys Solids 2006;54:2569–91.

[68] Hanaor DA, Gan Y, Einav I. Contact mechanics of fractal surfaces by spline assisted discretization. Int J Solids Struct 2015;59:121–31.

[69] Ciavarella M, Delfine V, Demelio V. A new 2D asperity model with interaction for studying the contact of multiscale rough random profiles. Wear 2006;261:556–67.

[70] Popov VL. Contact mechanics and friction. Berlin: Springer-Verlag; 2010.

[71] Komvopoulos K. Effects of multi-scale roughness and frictional heating on solid body contact deformation. Comptes Rendus Mécanique 2008;336:149–62.

[72] He G, Müser MH, Robbins MO. Adsorbed layers and the origin of static friction. Science 1999;284:1650–2.

[73] Krim J. Surface science and the atomic-scale origins of friction: what once was old is new again. Surf Sci 2002;500:741–58.

[74] Volokitin A, Persson B. Quantum field theory of van der Waals friction. Phys Rev B 2006;74:205413.

[75] Grzemba B. Modeling of a creep process between rough surfaces under tangential loading. Phys Mesomech 2014;17:223–7.

[76] Grzemba B, Pohrt R, Teidelt E, Popov VL. Maximum micro-slip in tangential contact of randomly rough self-affine surfaces. Wear 2014;309:256–8.

[77] Nosonovsky M, Bhushan B. Multiscale friction mechanisms and hierarchical surfaces in nano-and bio-tribology. Mater Sci Eng R: Rep 2007;58:162–93.

[78] Boitnott G, Biegel R, Scholz C, Yoshioka N, Wang W. Micromechanics of rock friction 2: quantitative modeling of initial friction with contact theory. J Geophys Res 1992;97:8965–78.

[79] Sokoloff J. Theory of the effects of multiscale surface roughness and stiffness on static friction. Phys Rev E 2006;73:016104.

[80] Rostami A, Streator JL. Study of liquid-mediated adhesion between 3D rough surfaces: a spectral approach. Tribol Int 2015;84:36–47.

[81] Hanaor DA, Gan Y, Einav I. Effects of surface structure deformation on static friction at fractal interfaces. Geotech Lett 2013;3:52–8.

[82] Li Q, Kim KS. Micromechanics of friction: effects of nanometre-scale roughness. Proc R Soc A: Math Phys Eng Sci 2008;464:1319–43.

[83] Streator JL. A model of liquid-mediated adhesion with a 2D rough surface. Tribol Int 2009;42:1439–47.

[84] Lovell M, Deng Z. Characterization of interfacial friction in coated sheet steels: influence of stamping process parameters and wear mechanisms. Tribol Int 2002;35:85–95.

[85] Perni S, Prokopovich P. Multi-asperity elliptical JKR model for adhesion of a surface with non-axially symmetric asperities. Tribol Int 2015;88:107–14.

[86] Pohrt R, Popov VL, Filippov AE. Normal contact stiffness of elastic solids with fractal rough surfaces for one-and three-dimensional systems. Phys Rev E 2012;86:026710.

[87] Sahoo P, Ghosh N. Finite element contact analysis of fractal surfaces. J Phys D: Appl Phys 2007;40:4245.

[88] Yastrebov VA, Durand J, Proudhon H, Cailletaud G. Rough surface contact analysis by means of the Finite Element Method and of a new reduced model. Comptes Rendus Mécanique 2011;339:473–90.

[89] Erlandsson R, Hadziioannou G, Mate CM, McClelland G, Chiang S. Atomic scale friction between the muscovite mica cleavage plane and a tungsten tip. J Chem Phys 1988;89:5190–3.

[90] Harrison JA, White CT, Colton RJ, Brenner DW. Atomistic simulations of friction at sliding diamond interfaces. MRS Bull 1993;18:50–3.

[91] Zappone B, Rosenberg KJ, Israelachvili J. Role of nanometer roughness on the adhesion and friction of a rough polymer surface and a molecularly smooth mica surface. Tribol Lett 2007;26:191–201.

[92] Svahn F, Kassman-Rudolphi e, Wallen E. The influence of surface roughness on friction and wear of machine element coatings. Wear 2003;254:1092–8.

[93] Mainsah E, Greenwood JA, Chetwynd D. Metrology and properties of engineering surfaces. Springer; 2001.

[94] Jolic K, Nagarajah C, Thompson W. Non-contact, optically based measurement of surface roughness of ceramics. Meas Sci Technol 1994;5:671.

[95] Paggi M, Pohrt R, Popov VL. Partial-slip frictional response of rough surfaces. Sci Rep 2014;4:5178.

[96] Goedecke A, Jackson RL, Mock R. Asperity creep under constant force boundary conditions. Wear 2010;268:1285–94.

[97] Sevostianov I, Kachanov M. Contact of rough surfaces: a simple model for elasticity, conductivity and cross-property connections. J Mech Phys Solids 2008;56:1380–400.

[98] Izquierdo S, López C, Valdés J, Miana M, Martínez F, Jiménez M. Multiscale characterization of computational rough surfaces and their wear using self-affine principal profiles. Wear 2012;274:1–7.

[99] Gosvami NN, Filleter T, Egberts P, Bennewitz R. Microscopic friction studies on metal surfaces. Tribol Lett 2010;39:19–24.

[100] Sundararajan S, Bhushan B. Static friction and surface roughness studies of surface micromachined electrostatic micromotors using an atomic force/friction force microscope. J Vac Sci Technol A 2001;19:1777–85.